TPX2, A Novel *Xenopus* MAP Involved in Spindle Pole Organization

Torsten Wittmann,* Matthias Wilm,‡ Eric Karsenti,* and Isabelle Vernos*

*Cell Biology and Cell Biophysics Program, ‡Biochemical Instrumentation Program, European Molecular Biology Laboratory, D-69117 Heidelberg, Germany

Abstract. TPX2, the targeting protein for *Xenopus* kinesin-like protein 2 (Xklp2), was identified as a microtubule-associated protein that mediates the binding of the COOH-terminal domain of Xklp2 to microtubules (Wittmann, T., H. Boleti, C. Antony, E. Karsenti, and I. Vernos. 1998. *J. Cell Biol.* 143:673–685). Here, we report the cloning and functional characterization of *Xenopus* TPX2. TPX2 is a novel, basic 82.4-kD protein that is phosphorylated during mitosis in a microtubule-dependent way. TPX2 is nuclear during interphase and becomes localized to spindle poles in mitosis. Spindle pole localization of TPX2 requires the activity of the dynein–dynactin complex. In late anaphase TPX2 becomes relocalized from the spindle poles to the midbody. TPX2 is highly homologous to a human protein of unknown function and thus defines a new family of vertebrate spindle pole components. We investigated the function of TPX2 using spindle assembly in *Xenopus* egg extracts. Immunodepletion of TPX2 from mitotic egg extracts resulted in bipolar structures with disintegrating poles and a decreased microtubule density. Addition of an excess of TPX2 to spindle assembly reactions gave rise to monopolar structures with abnormally enlarged poles. We conclude that, in addition to its function in targeting Xklp2 to microtubule minus ends during mitosis, TPX2 also participates in the organization of spindle poles.

Key words: spindle pole • microtubules • dynein–dynactin • TPX2 • Xklp2

Introduction

Once during the cell cycle, chromosomes are segregated by a bipolar microtubule-based structure, the mitotic spindle. Spindles consist of two antiparallel arrays of microtubules. The microtubule minus ends are focused into the two spindle poles, whereas their plus ends overlap in the equatorial region. Spindle assembly and chromosome segregation depend on the function of a variety of microtubule motor proteins including kinesin-like proteins (KLPs)[1] and cytoplasmic dynein (for recent reviews see Endow, 1999; Heald and Walczak, 1999; Heck, 1999; Vernos and Karsenti, 1996). In addition, microtubule-associated proteins (MAPs) are required for the regulation of microtubule dynamics (reviewed by Andersen, 2000; Cassimeris, 1999) and other molecules, like the small GTPase Ran, are involved in microtubule polymerization during mitosis (Carazo-Salas et al., 1999; Kalab et al., 1999; Wilde and Zheng, 1999).

Many proteins including motors, MAPs, protein kinases, and phosphatases, as well as centrosome components become enriched at spindle poles during mitosis. In many cases both the significance of this localization and the mechanism by which these proteins reach the poles during mitosis are not well understood. Minus end–directed motor proteins like cytoplasmic dynein and XCTK2 (Walczak et al., 1997) may accumulate at microtubule minus ends simply as a consequence of their motor activity and directly transport other proteins to the poles. Indeed, dynein forms a complex with dynactin and NuMA in *Xenopus* egg extracts, suggesting that it directly transports NuMA to the poles (Merdes et al., 2000). In addition, all of these proteins are required for the formation of a focused spindle pole (Gaglio et al., 1995, 1997; Heald et al., 1996, 1997; Merdes et al., 1996). Other microtubule-dependent mechanisms by which proteins accumulate at the spindle poles have not yet been demonstrated but they may involve interactions with proteins actively transported to the poles earlier or depend on the poleward flux of spindle microtubules (Waterman-Storer et al., 1998; Sawin and Mitchison, 1991b). In addition, there appear to be entirely different

The online version of this article contains supplemental material.

Address correspondence to Isabelle Vernos, European Molecular Biology Laboratory, Cell Biology and Cell Biophysics Program, D-69117 Heidelberg, Germany. Tel.: 49 6221 387 342. Fax: 49 6221 387 512. E-mail: vernos@embl-heidelberg.de

[1] *Abbreviations used in this paper:* cdc2 kinase, cyclin-dependent kinase 2; CSF, cytostatic factor; GFP, green fluorescent protein; GST, glutathione-*S*-transferase; KLP(s), kinesin-like protein(s); MAP(s), microtubule-associated protein(s); MAP kinase, mitogen-activated protein kinase; TPX2, targeting protein for Xklp2; Xklp2, *Xenopus* kinesin-like protein 2.

mechanisms for the recruitment of spindle pole proteins. γ-Tubulin, for example, as well as the *Drosophila* centrosomal proteins CP60 and CP190 accumulate at the spindle poles at the onset of mitosis in a microtubule-independent way (Oegema et al., 1995; Khodjakov and Rieder, 1999).

We have previously identified a *Xenopus* kinesin-like protein, Xklp2, that contains an NH_2-terminal motor domain and is a plus end–directed microtubule motor. Nevertheless, Xklp2 accumulates at the minus ends of spindle microtubules during mitosis (Boleti et al., 1996; Wittmann et al., 1998). Spindle pole targeting information resides in the COOH-terminal domain of Xklp2. Using a glutathione-*S*-transferase (GST) fusion protein containing the COOH-terminal 250 amino acids of Xklp2, GST-Xklp2-Tail, we previously examined the mechanism of Xklp2 localization to the poles. In addition to the function of the dynein–dynactin complex, the localization of GST-Xklp2-Tail requires a MAP, TPX2 (targeting protein for Xklp2), that we purified from *Xenopus* egg extract based on its ability to mediate the binding of GST-Xklp2-Tail to pure microtubules (Wittmann et al., 1998).

To learn more about the function and localization of proteins at the mitotic spindle pole, we now describe the molecular cloning and functional characterization of TPX2. TPX2 is a novel MAP that defines a new class of vertebrate spindle pole components and is itself localized to spindle poles in a dynein-dependent way. We also show that in addition to its function in localizing Xklp2 to microtubule minus ends, TPX2 plays an important role in spindle pole organization.

Materials and Methods

Protein Sequencing

TPX2 was purified as described (Wittmann et al., 1998) up to the Mono S chromatography step. The protein was in-gel digested with trypsin in a buffer containing 33% ^{18}O water to partially label the COOH termini of the peptides. The peptides were extracted and desalted on a Poros R2 column assembled in a pulled glass capillary (Shevchenko et al., 1996). The total peptide mixture was eluted in 2 μl 60% methanol, 5% formic acid into a gold-coated nanoelectrospray glass capillary, and analyzed on an API III triple quadrupole mass spectrometer (PE-Sciex; Wilm and Mann, 1996). For every peptide, two fragment spectra were acquired, the first selecting the entire $^{16}O/^{18}O$ isotopic envelope of the peptide for fragmentation and a second selecting only the ^{18}O isotopes. Sequences were determined by identifying the COOH-terminal y-ions throughout the fragment spectrum via their $^{16}O/^{18}O$ isotopic pattern and their different isotopic representation in both spectra. The mass differences between two adjacent y-ions correspond to a single amino acid. Several pairs of amino acids can not be distinguished due to their identical or close to identical mass (I/L and K/Q).

Cloning of TPX2

mRNA was isolated from total *Xenopus* egg RNA using the PolyATract mRNA Isolation System (Promega) and first strand cDNA was synthesized with SuperScript II reverse transcriptase (GIBCO BRL) according to standard protocols. Using the peptide sequences degenerate oligonucleotides containing up to four inosines (19–26 nucleotides, 256–576–fold degeneracy) were synthesized and used for PCR reactions with all possible primer combinations.

Two different PCR products were used to screen a mature *Xenopus* oocyte cDNA library in λ-ZAP (from John Shuttleworth, University of Birmingham, UK). Library screening, Northern blots and all subsequent cloning was done according to standard protocols (Ausubel et al., 1995). Several independent clones were isolated and exonuclease III deletions of the longest clone (3.5 kb) were sequenced on both strands by the EMBL sequencing service.

Recombinant Proteins

Untagged recombinant TPX2 was produced using the IMPACT T7 one-step protein purification system (New England Biolabs Inc.). The TPX2 open reading frame was amplified by PCR with PfuTurbo DNA polymerase (Stratagene) using 10 cycles of amplification introducing an NcoI and a XmaI site at its 5′- and 3′-end, respectively, and cloned into the pTYB4 vector (New England Biolabs, Inc.) such that after cleavage only an additional proline and a glycine residue would remain at the COOH terminus of the recombinant TPX2. The protein was expressed in *E. coli* BL21(DE3)pLysS cells, purified and cleaved on a chitin column according to the manufacturer's instructions, dialyzed against 25 mM K-Hepes, pH 7.5, 250 mM KCl, 2 mM $MgCl_2$, 10% glycerol, and 1 mM DTT, frozen in liquid nitrogen, and stored at −80°C.

GST-TPX2 fusion proteins were generated containing either the full-length TPX2 protein or the NH_2-terminal 431 amino acids. BamHI and SalI restriction sites were introduced by PCR and the fragments were cloned into the pGEX-4T-1 vector (Amersham Pharmacia Biotech). GST-fusion proteins were expressed and purified by glutathione affinity chromatography according to standard protocols.

To obtain a green fluorescent protein (GFP) TPX2 fusion protein, the TPX2 cDNA was amplified by PCR introducing EcoRI and BamHI restriction sites and the fragment was cloned into a modified pHAT2 vector that contained the EGFP sequence after the histidine tag (obtained from Andrei Popov, EMBL, Heidelberg, Germany). The histidine-tagged GFP-TPX2 was expressed in *E. coli* BL21(DE3)pLysS cells and purified native on TALON metal affinity resin (CLONTECH Laboratories, Inc.) according to the manufacturer's instructions. Purified GFP-TPX2 was dialyzed, frozen, and stored the same way as untagged TPX2.

p50/dynamitin was produced as described (Wittmann and Hyman, 1999).

Egg Extracts, Spindle Assembly and Immunodepletions

Cytostatic factor arrested extracts (CSF-extracts) were prepared according to Murray (1991). However, energy mix was omitted in many experiments since it did not appear to improve the quality of the extracts significantly. For cycled spindle assembly, rhodamine-labeled tubulin (Hyman et al., 1991) was added at 0.2 mg/ml and sperm at a concentration of ~500 nuclei/μl to 15–20 μl CSF-extract and the extract was released into interphase by the addition of 0.4 mM Ca^{2+} (Heald et al., 1998; Desai et al., 1999). The reactions were incubated for 80–90 min at 20°C and cycled back to mitosis by the addition of one volume of CSF-extract. After 1 h, the spindles were fixed in 1 ml BRB80 (80 mM K-Pipes, pH 6.8, 1 mM EGTA, 1 mM $MgCl_2$) containing 30% glycerol, 0.25% glutaraldehyde, and 0.1% Triton X-100 and subsequently centrifuged (HB4 rotor, 12,000 rpm, 12 min, 16°C) through a 40% glycerol cushion in BRB80 onto poly-L-lysine–coated coverslips as described (Sawin and Mitchison, 1991a).

For immunodepletions, 7 μg of antibody was bound to 25 μl of protein A–conjugated Dynabeads 280 (Dynal). The antibody was mixed with the beads in a total volume of 100–200 μl PBS containing 0.1% Triton X-100 and incubated for at least 1 h on a rotating wheel. The beads were then washed once with PBS, 0.1% Triton X-100, once with 0.5 M NaCl in PBS, 0.1% Triton X-100, and three times with CSF-XB (10 mM K-Hepes, pH 7.7, 50 mM sucrose, 100 mM KCl, 2 mM $MgCl_2$, 0.1 mM $CaCl_2$, and 5 mM EGTA). Between washing steps the beads were retrieved on a magnet and at the end the buffer was removed as much as possible. 100 μl extract was added to the beads and pipetted up and down carefully until the beads were completely resuspended. The extract was then placed on ice for 90 min and mixed by pipetting once or twice during this time. The beads were retrieved on a magnet on ice for ~10 min and the recovered extract was used for spindle assembly.

To analyze bound proteins, the beads were washed three times with CSF-XB, three times with PBS, 0.1% Triton X-100, boiled in SDS-PAGE sample buffer and subjected to gel electrophoresis. Alternatively, TPX2-associated proteins were eluted with 0.5 M NaCl in PBS and 0.1% Triton X-100 for 15 min on ice before SDS-PAGE.

Immunofluorescence, Transfections, and Microscopy

XL177 cells grown on coverslips were briefly rinsed with 70% PBS and fixed in methanol at −20°C for 5 min. Antibodies were diluted in PBS

containing 0.1% Triton X-100 and 2% BSA. Primary and secondary antibodies were applied to the coverslips for 20 min at room temperature, coverslips were washed in between incubations with PBS for at least three times and finally embedded in mowiol (Hoechst). Pictures were taken with an LSM 510 confocal microscope (ZEISS).

The TPX2 cDNA sequence was amplified by PCR introducing an EcoRI and a BamHI restriction site and cloned into the pEGFP-N1 eukaryotic expression vector (CLONTECH Laboratories, Inc.). XL177 cells were transfected by electroporation essentially as described (Tuma et al., 1998). In brief, XL177 cells were electroporated in 0.2-cm cuvettes at 220 V, 200 Ω, and 250 μF using a GenePulser II (Bio-Rad Laboratories). After electroporation the cells were directly plated onto poly-L-lysine–coated coverslips and mitotic transfected cells were observed 30–60 h after transfection.

Spindles assembled in egg extract were processed for immunofluorescence as described (Wittmann et al., 1998). All pictures of in vitro assembled structures were taken with a 12-bit grayscale cooled CCD camera (F-View, Soft Imaging System) mounted on an Axioskop-2 (ZEISS) and digital images were processed with the analysis software (Soft Imaging System) and Adobe Photoshop. For quantification, images were taken at 16× magnification, printed, and the structures were scored from the printouts. For fluorescence intensity measurements, images were taken at 63× magnification with identical camera and illumination settings below saturation of the camera. The gray values of all pixels in a 50 × 50–pixel area were integrated and a background value was subtracted determined from an equal-sized square on the same image.

Rabbit polyclonal antibodies were raised against the GST-TPX2 fusion proteins. The antibodies were affinity-purified on a column of untagged TPX2 covalently linked to Sepharose. Anti-GST and anti-Xklp2 antibodies were as described (Wittmann et al., 1998). Monoclonal anti–α-tubulin antibodies were from Amersham. Fluorescent- and horseradish peroxidase–conjugated antibodies were from Jackson ImmunoResearch Laboratories, Amersham Pharmacia Biotech (CyDye), and Molecular Probes (Alexa).

Microtubule Sedimentation Assay and In Vitro Phosphorylation

Purified tubulin was polymerized as described (Wittmann et al., 1998), mixed with recombinant proteins in 100 μl 20 mM K-Hepes, pH 7.5, 200 mM KCl, 2 mM $MgCl_2$, 1 mM EGTA, 0.1% Triton X-100, 1 mM DTT, and 10 μM taxol and incubated for 20 min at 20°C. The reactions were then centrifuged through a 10% sucrose cushion in BRB80 as described (Wittmann et al., 1998) and analyzed by SDS-PAGE and immunoblot. GFP-TPX2 fluorescence was measured in a Luminescence Spectrometer (Aminco Bowman). In microtubule sedimentation assays with crude egg extract, the reactions were diluted 1:5 in the above buffer before centrifugation.

For phosphorylation in egg extract, ~50 μCi γ-[^{32}P]ATP (Amersham Pharmacia Biotech) was added to 50 μl mitotic or interphase *Xenopus* egg extract and incubated for 20 min at 20°C. The reaction was stopped by the addition of 200 μl stop buffer (100 mM NaF, 80 mM β-glycerophosphate, 20 mM $Na_4P_2O_7$, 20 mM EDTA, 2 μM microcystin, and 10 μg/ml aprotinin, pepstatin, leupeptin, pH 7.5) containing 5 μg anti-TPX2 antibody bound to AffiPrep protein A beads (Bio-Rad Laboratories). The mixture was incubated for 1 h on a rotating wheel at 4°C, the beads were washed twice with stop buffer and twice with PBS containing 0.1% Triton X-100 and analyzed by SDS-PAGE and autoradiography. The degree of radioactivity incorporation was quantified with a PhosphorImager (Fuji).

Online Supplemental Material

Time-lapse imaging of a mitotic XL177 cell expressing low levels of GFP-TPX2 as shown in Fig. 4 B. The sequence contains images taken every minute over a total time of 60 min. Supplemental materials are viewable at http://www.jcb.org/cgi/content/full/149/7/1405/DC1.

Results

Molecular Characterization of TPX2

TPX2 was purified from mitotic *Xenopus* egg extract as described (Wittmann et al., 1998) and peptide sequences of several tryptic fragments were obtained by mass spectrometry. A full-length cDNA clone was isolated by degenerate PCR and screening of a *Xenopus laevis* oocyte cDNA library. The PCR fragment used for library screening hybridized with a single transcript of ~3 kb on a Northern blot of total *Xenopus* egg RNA (Fig. 1 A).

The longest TPX2 cDNA clone contained an open reading frame encoding a polypeptide of 715 amino acids (Fig. 1 B). The predicted molecular mass is 82.4 kD and thus slightly lower than the apparent size of ~100 kD observed during the initial purification from egg extract. The protein is highly charged (18.7% strongly basic and 14.7% strongly acidic amino acids) and very basic with a predicted isoelectric point of ~9.5.

Database searches with either the nucleotide or the predicted protein sequence did not identify any homologous protein with known function. However, the TPX2 protein sequence was homologous to a number of vertebrate ESTs

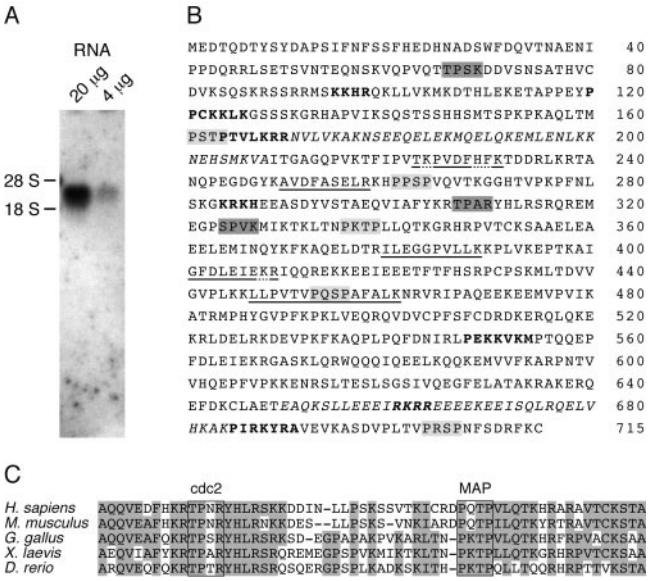

Figure 1. Molecular cloning of TPX2. (A) Northern blot of total *Xenopus* egg RNA hybridized with a PCR fragment obtained in a reaction with degenerate oligonucleotides designed according to TPX2 peptide sequences. The amount of RNA loaded per lane is indicated on top. The migration position of the 28S rRNA (4,115 nucleotides) and the 18S rRNA (1,826 nucleotides) is shown on the left. The probe recognizes a unique transcript of 3.0–3.5 kb. (B) Amino acid sequence of TPX2. Peptide sequences obtained by mass spectrometry are underlined. Differences between the predicted protein sequence and the peptide sequences are indicated by dotted underlines. Putative cdc2 kinase sites, (S/T)PX(K/R), are shaded in dark gray and MAP kinase phosphorylation sites, PX(S/T)P, are shaded in light gray, nuclear localization signals are shown in bold and the predicted coiled-coil regions are in italics. The complete cDNA sequence of *Xenopus laevis* TPX2 is available from GenBank/EMBL/DDBJ under accession number AF244546. (C) Sequence comparison of a region from TPX2 (corresponding to amino acids 297–356) with the human protein fls353 (amino acids 328–387) and predicted protein sequences from ESTs from mouse, chicken and zebrafish (these data are available from GenBank/EMBL/DDBJ under accession number AI415194, AJ394859, and AI883915). Conserved residues are shaded in gray and boxes indicate the highly conserved cdc2 and MAP kinase phosphorylation sites within this region.

and highly similar to a hypothetical human 747–amino acid protein (fls353 or DIL-2, respectively; these data are available from GenBank/EMBL/DDBJ under accession number AB024704 and AB027467; see also Fig. 1 C). TPX2 and fls353 are 52% identical over the whole protein sequence. The degree of identity increases to 63% when the NH_2-terminal 180 amino acids are not considered.

Analysis of the TPX2 amino acid sequence revealed that it contained three putative cdc2 phosphorylation sites as well as five putative sites for phosphorylation by MAP kinase. Most of these phosphorylation sites were conserved between the frog and human protein. The TPX2 protein also contained seven potential nuclear localization signals and two short regions (amino acids 171–208 and 650–684) that showed a significant probability for coiled-coil formation.

To investigate the function of TPX2 we raised polyclonal antibodies against the full-length protein, anti-TPX2, and against the NH_2-terminal 431 amino acids, anti-TPX2N. Both affinity-purified antibodies recognized a single protein band of ~100 kD in mitotic as well as in interphase *Xenopus* egg extracts, in MAPs purified from mitotic egg extract and in a lysate prepared from unsynchronized *Xenopus* tissue culture cells (Fig. 2 A). In mitotic egg extract and in the mitotic MAPs fraction the TPX2 band was slightly upshifted indicating a posttranslational modification during mitosis.

To test whether this upshift was due to phosphorylation, TPX2 was immunoprecipitated from interphase and mitotic extract after incubation with radiolabeled ATP (Fig. 2 B). The protein immunoprecipitated from mitotic extract showed a retardation in gel electrophoresis and a three- to fivefold increased incorporation of radioactivity indicating that it was more phosphorylated in mitotic compared with interphase extract. Interestingly, additional phosphorylation events were observed only in mitotic but not in interphase extract upon microtubule polymerization. Addition of taxol to mitotic extract caused a further upshift of the TPX2 band and another two- to threefold increase in incorporation of radioactivity. These results show that TPX2 can be phosphorylated in mitotic extract on several phosphorylation sites in distinct steps.

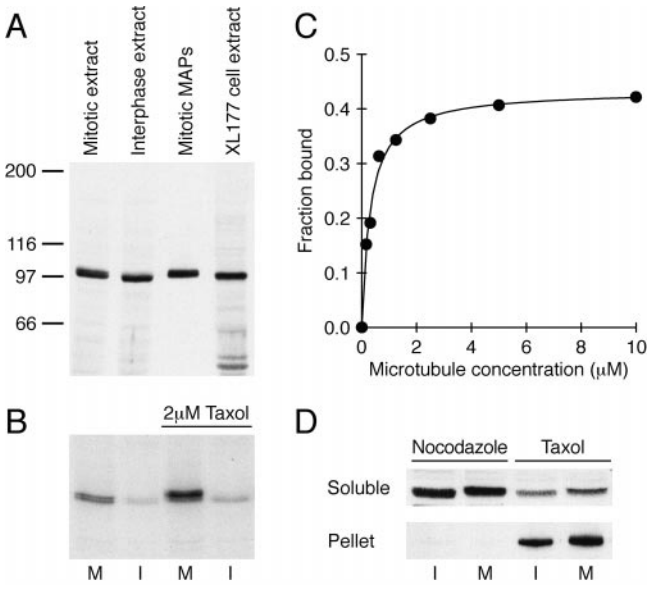

Figure 2. TPX2 is phosphorylated in mitotic egg extract and binds to microtubules with high affinity. (A) Immunoblot of low-speed *Xenopus* egg extracts, mitotic microtubule-associated proteins purified as described (Wittmann et al., 1998) and XL177 SDS lysate probed with affinity-purified anti-TPX2N. The molecular mass of marker proteins is indicated on the left. (B) Phosphorylation of TPX2 in mitotic, M, and interphase, I, egg extract incubated in the presence of γ-[^{32}P]ATP. Taxol was added to 2 μM and the extracts were incubated for 30 min at 20°C. The immunoprecipitates were analyzed on a 6% SDS-PAGE and subjected to autoradiography. TPX2 is phosphorylated in mitotic extract and hyperphosphorylated upon assembly of microtubules. (C) Microtubule sedimentation assay of GFP-TPX2 with pure microtubules. The fraction of GFP-TPX2 bound to microtubules is plotted versus the microtubule concentration. The solid line represents the hyperbolic curve fit. (D) Microtubule sedimentation assay from crude extract. Interphase, I, and mitotic, M, extract were supplemented with either 20 μM nocodazole or 2 μM taxol, incubated for 20 min at 20°C and centrifuged through a 10% sucrose cushion. The immunoblots show the amount of TPX2 present in equivalent amounts of the soluble and pelleted fraction.

TPX2 Binds to Microtubules with High Affinity

To estimate the affinity of TPX2 for microtubules, bacterially expressed GFP-TPX2 was mixed with different concentrations of pure, prepolymerized microtubules. The microtubule-bound fraction was removed by centrifugation, and the amount of GFP-TPX2 that remained soluble was determined by fluorescence spectrometry. Plotting of the fraction of GFP-TPX2 bound to microtubules versus the microtubule concentration and direct hyperbolic curve fitting yielded a dissociation constant of below 0.5 μM (Fig. 2 C). However, even with saturating amounts of microtubules only about half of the GFP fluorescence was recovered in the microtubule pellet which is probably due to the relatively high amount of truncated GFP-TPX2 present in the protein preparation (see Fig. 3 B, last lane).

Since TPX2 was phosphorylated in a cell cycle–dependent manner, we analyzed whether the cell cycle state of the extract affected the association of TPX2 with microtubules. Interphase and mitotic egg extract were incubated in the presence of either nocodazole or taxol, and the insoluble proteins were recovered by centrifugation through a sucrose cushion (Fig. 2 D). Regardless of the cell cycle state of the extract, the major amount of TPX2 was recovered in the microtubule pellet. This suggests that global cell cycle–dependent phosphorylation does not regulate the affinity of TPX2 for microtubules.

TPX2 Is Required for the Targeting of Xklp2 to Microtubule Minus Ends

To verify that the protein we have cloned was sufficient for the binding of the COOH-terminal domain of Xklp2 to microtubules we used a sedimentation assay with pure, prepolymerized microtubules. Microtubules were mixed with bacterially expressed TPX2 and GST-Xklp2-Tail and centrifuged through a sucrose cushion (Fig. 3 A). In the absence of microtubules both TPX2 and GST-Xklp2-Tail

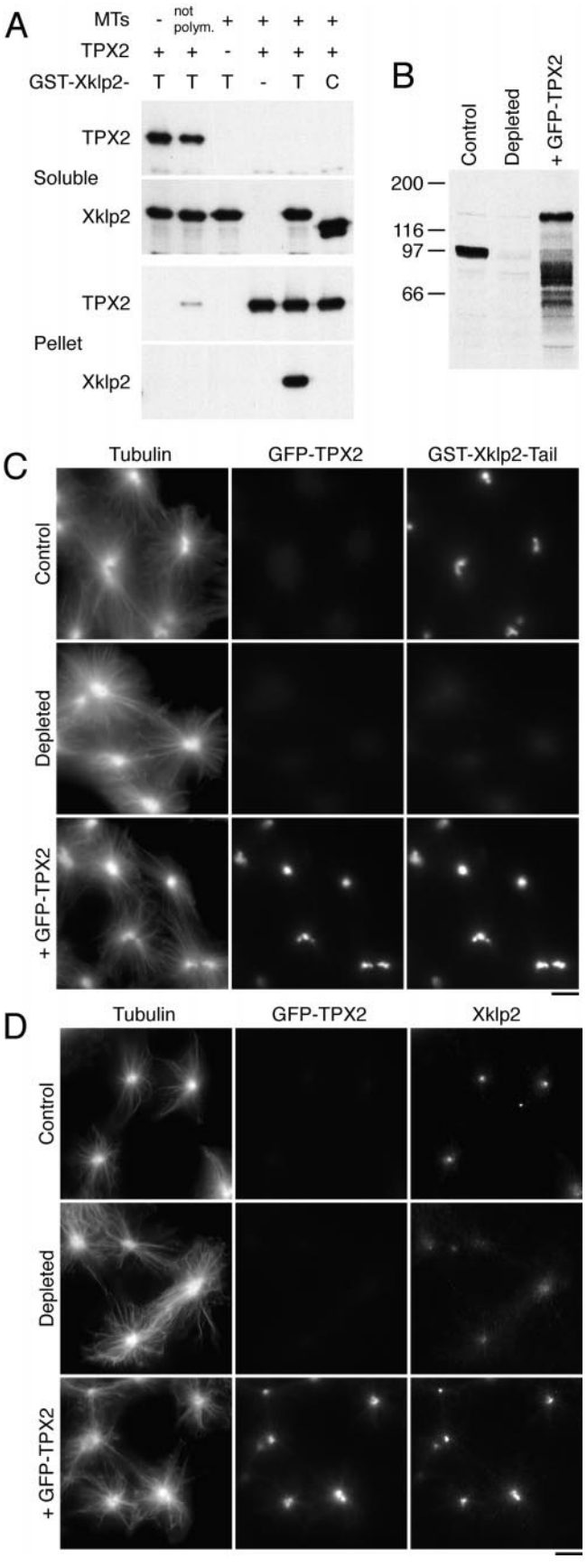

Figure 3. TPX2 is required for the binding of Xklp2 to microtubules. (A) Microtubule sedimentation assay. Pure prepolymerized microtubules (1 μM) were mixed with bacterially expressed TPX2 and GST-Xklp2-Tail (both 0.1–0.2 μM), T, or GST-Xklp2-CDel2, C (Wittmann et al., 1998), as indicated on top, incubated for 20 min at 20°C and centrifuged through a 10% sucrose cushion. Equivalent amounts of the soluble and pelleted fraction were analyzed by immunoblot probed with anti-TPX2N or anti-Xklp2 antibodies as indicated. GST-Xklp2-Tail is only recovered in the pellet in the presence of both microtubules and TPX2. (B) Immunodepletion of TPX2 and GFP-TPX2 addback. 1-μl aliquots of extract were analyzed by immunoblot and probed with anti-TPX2N. The molecular mass of marker proteins is indicated on the left. Additional bands in the addback lane are due to degradation products of GFP-TPX2. (C) Mitotic asters assembled for 30 min at 20°C in the presence of 5% DMSO, 1 μM GST-Xklp2-Tail, and rhodamine-labeled tubulin in control- and TPX2-depleted extract supplemented with bacterially expressed GFP-TPX2. The asters were sedimented onto coverslips and stained with an anti-GST and an Alexa350-conjugated anti–rabbit antibody. (D) Mitotic asters assembled in the presence of Cy5-labeled tubulin as in C but without GST-Xklp2-Tail added. The asters were stained with an anti-Xklp2 and a rhodamine-conjugated anti–rabbit antibody. Bars, 10 μm.

remained soluble. However, in the presence of microtubules, TPX2 was quantitatively recovered in the microtubule pellet. GST-Xklp2-Tail cosedimented with microtubules only when TPX2 was included in the reaction (Fig. 3 A, lane 5). The specificity of this interaction was further demonstrated by the observation that a truncated version of GST-Xklp2-Tail that does not localize to mitotic structures (Wittmann et al., 1998) did not cosediment with microtubules in the presence of TPX2 (Fig. 3 A, last lane). The minor amount of TPX2 that pelleted in the presence of unpolymerized tubulin was probably due to some tubulin aggregation (Fig. 3 A, second lane).

The above results confirmed that TPX2 was required to bind the COOH-terminal domain of Xklp2 to microtubules. However, in our previous work we could not determine whether TPX2 was required for targeting Xklp2 to microtubule minus ends in mitotic egg extracts. To address this question we used the anti-TPX2N antibody to deplete the protein from extract and analyzed the localization of Xklp2 in mitotic asters assembled by the addition of DMSO (Stearns and Kirschner, 1994). DMSO-induced asters formed both in control and TPX2 extracts (Fig. 3). However, in TPX2-depleted extract GST-Xklp2-Tail failed to localize to the center of these asters, whereas it did localize perfectly well in control-depleted extracts. GFP-TPX2 added to the TPX2-depleted extract became localized to the center of the asters and rescued the localization of GST-Xklp2-Tail (Fig. 3 C). The endogenous Xklp2 showed essentially the same behavior as exogenously added GST-Xklp2-Tail (Fig. 3 D).

TPX2 Is Localized to Mitotic Spindle Poles

We next determined the localization of TPX2 both in *Xenopus* tissue culture cells and in spindles assembled in vitro. During interphase a small subset of cells displayed very faint nuclear staining. No localization was observed along interphase microtubules (Fig. 4). During prophase, TPX2 staining became apparent at the center of the mitotic asters around the time of nuclear envelope break-

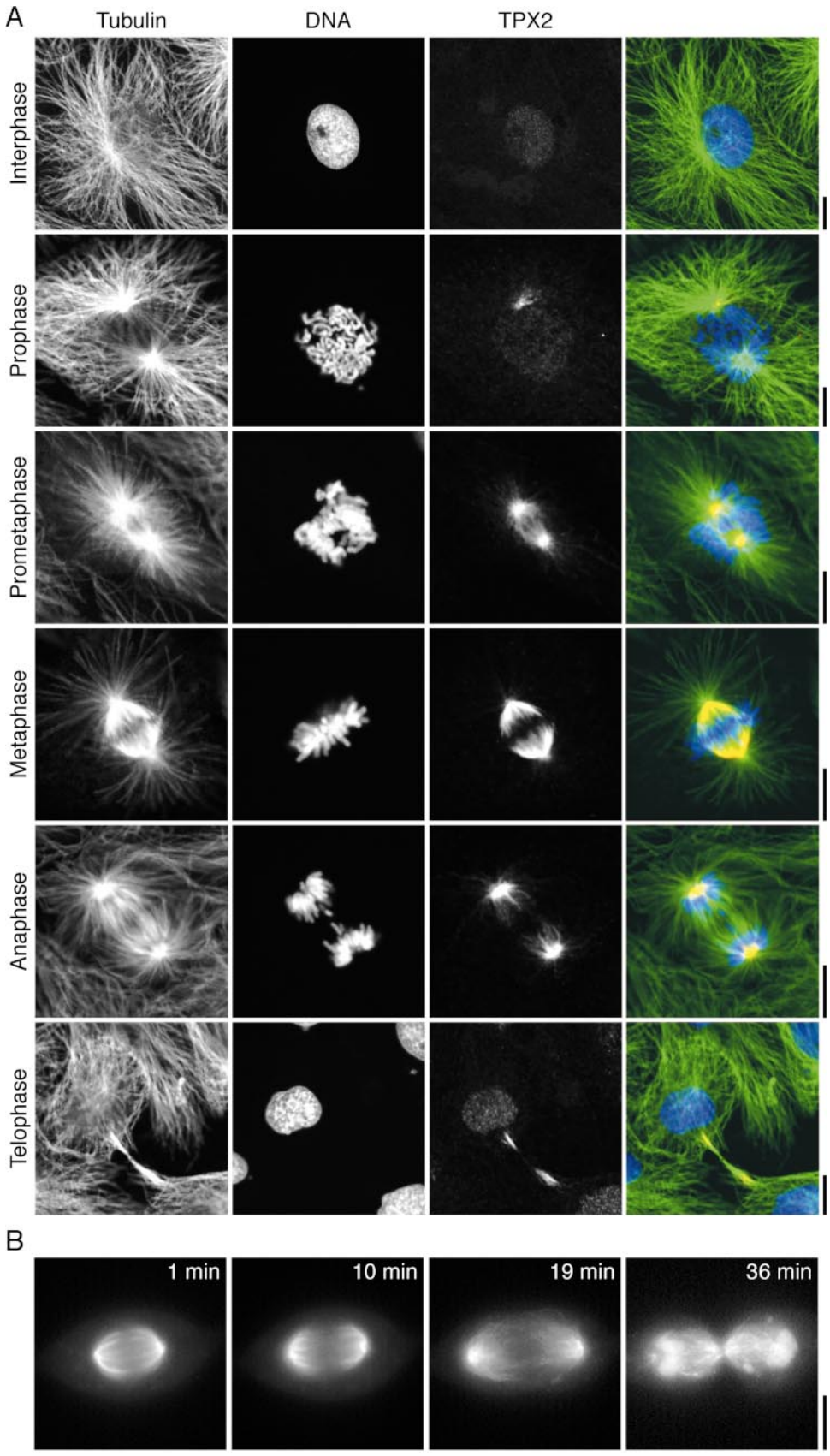

Figure 4. (A) Immunolocalization of TPX2 throughout the cell cycle. XL177 *Xenopus* tissue culture cells were fixed in cold methanol and stained with 0.6 μg/ml affinity-purified anti-TPX2N, monoclonal anti-tubulin, and Hoechst 33258 followed by FITC-labeled anti–mouse and TRITC-labeled anti–rabbit antibodies. Images represent single confocal slices. The same staining pattern was observed with anti-TPX2 or when the cells were fixed with glutaraldehyde. TPX2 staining appears at the end of prophase, persists at the spindle poles throughout mitosis until late anaphase. It then relocalizes to the midbody where it disappears in late telophase. (B) Live images of a mitotic XL177 cell expressing low amounts of GFP-TPX2. Note the nuclear fluorescence in telophase. The elapsed time is indicated in the upper right corner. Supplemental video is viewable at http://www.jcb.org/cgi/content/full/149/7/1405/DC1. Bars, 10 μm.

down and in prometaphase the center of both asters was labeled. The labeling intensity increased until metaphase and spindle microtubules were brightly stained. The signal appeared to be more intense towards the spindle poles and astral microtubules were almost unlabeled. At the onset of anaphase, TPX2 remained concentrated at the spindle poles. In late anaphase, a relocalization to the midzone occurred that resulted in a fairly strong staining of the midbody so that in late telophase no staining was left in the centrosome area (Fig. 4).

Since TPX2 was present in comparable amounts both in mitotic and in interphase egg extract we performed immunofluorescence on in vitro interphase nuclei and on spindles assembled in interphase-to-mitotic extracts (Sawin and Mitchison, 1991a). In interphase extract, TPX2 showed a diffuse nuclear localization as well as an association with the nuclear envelope and a branched tubular structure within the nucleus. This staining became more prominent after longer incubation times when the chromatin started to condense (Fig. 5 A). Patches of condensing chromatin were in close proximity to the TPX2-labeled structures. This nuclear staining was not observed in TPX2-depleted extracts or with secondary antibodies alone. At very early time points (5–10 min) after cycling the extract back into mitosis we could observe half-spindle–like structures where microtubules had just begun to interact with the condensing chromatin. Interestingly, in these structures TPX2 staining was continuous between the remains of the nucleus and microtubules in the proximity of the chromatin (Fig. 5 B). After ~60 min, a high percentage of bipolar spindles had formed. In most spindles TPX2 was strongly concentrated in a crescent-shaped area at both spindle poles (Fig. 5 B). Similar spindle pole staining was observed in spindles assembled in the absence of centrosomes around chromatin beads (data not shown). To compare TPX2 localization to another well-characterized pole protein, spindles were assembled and fixed under identical conditions and then stained either for TPX2 or NuMA (Fig. 5 C). In contrast to NuMA, which was concentrated in a very small area at spindle poles, TPX2 was also present on microtubules throughout the spindle.

As an alternative way to examine the localization of TPX2, GFP-tagged TPX2 was either added to egg extracts or transfected into *Xenopus* tissue culture cells. In interphase and mitotic extracts, GFP-TPX2 showed the same behavior as the endogenous protein detected by immunofluorescence (data not shown). In transfected tissue culture cells, we could observe that GFP-TPX2 remained at the spindle poles until late anaphase. It then became redistributed to the midbody along spindle microtubules and was imported into the reforming nuclei (Fig. 4 B and video). Taken together, these results show that TPX2 exhibits a complex pattern of localization during the cell cycle.

TPX2 Localization Requires the Dynein–Dynactin Complex

Since we had observed that the localization of the GST-Xklp2-Tail protein was dependent on a functional dynein–dynactin complex (Wittmann et al., 1998) it was likely that TPX2-localization would also require this motor protein. To test this hypothesis, spindles were assembled in cycled mitotic extract and recombinant p50/dynamitin was added to the reactions when the extract was cycled back from interphase to mitosis. The addition of p50/dynamitin to egg extract leads to the dissociation of the dynactin complex (Wittmann and Hyman, 1999). Almost all of the bipolar structures formed had unfocused poles, a result expected when dynein is inhibited during spindle assembly (Heald et al., 1997). Moreover, spindles assembled in the presence of p50/dynamitin were ~30% longer than in the control reaction (in average 33 ± 3.0 μm versus 26 ± 3.6 μm, $n = 20$). In control spindles, TPX2 was concentrated close to the spindle poles. However, in the presence of p50/dynamitin, TPX2 staining was less bright and spread over the whole length of the spindle (Fig. 6 A). This observation was confirmed by measuring the TPX2 fluorescence intensity profile along the spindle axis. The two prominent peaks close to the spindle poles corresponding to the highest TPX2 concentration disappeared in the presence of p50/dynamitin and the intensity profile assumed a shape more similar to that of tubulin (Fig. 6 B). The total TPX2 fluorescence was reduced to ~70% compared with the control. In contrast, the total tubulin fluorescence remained roughly the same in p50/dynamitin-treated spindles and the intensity profile was only slightly elongated. This indicates that dynein–dynactin function is necessary for TPX2-localization to the spindle poles.

TPX2 Is Involved in Spindle Pole Organization

To further analyze the function of TPX2, we depleted the protein from egg extract and tested the effect on spindle assembly. In our hands, spindles assembled in extracts cycled from interphase to mitosis yielded more reproducible results and a higher percentage of bipolar spindles than half-spindle reactions in CSF extracts (Sawin and Mitchison, 1991a). However, published immunodepletion protocols most often resulted in extracts incapable of cycled spindle assembly (Desai et al., 1999). We therefore used protein A–conjugated magnetic beads and minimized the agitation of the extract during incubation to obtain depleted extracts that reliably formed bipolar spindles in cycled extracts. With this method, ~95% of TPX2 could be reproducibly removed from egg extract (see Fig. 8 A).

In addition to TPX2, a polypeptide of ~90 kD was recovered almost in stoichiometric amounts in TPX2 immunoprecipitations (Fig. 7). This protein could be eluted from the beads with a high salt buffer (Fig. 7 A) and was not recognized by anti-TPX2 antibodies demonstrating that it was not a TPX2 degradation product. Furthermore, when an excess of GST-TPX2 fusion protein was added to mitotic extract and immunoprecipitated with an anti-GST antibody, the 90-kD band was again recovered in stoichiometric amounts (Fig. 7 B). This indicates that the 90-kD protein may form a 1:1 complex with TPX2. Since the 90-kD protein appears to be more abundant in egg extract than TPX2 it seems unlikely that its amount is significantly reduced in TPX2-depleted extract. The identification and analysis of this protein will be the subject of future studies. By contrast, TPX2 did not coimmunoprecipitate with GST-TPX2. NuMA, subunits of the dynein–dynactin complex or Xklp2 could not be detected in TPX2 immunopre-

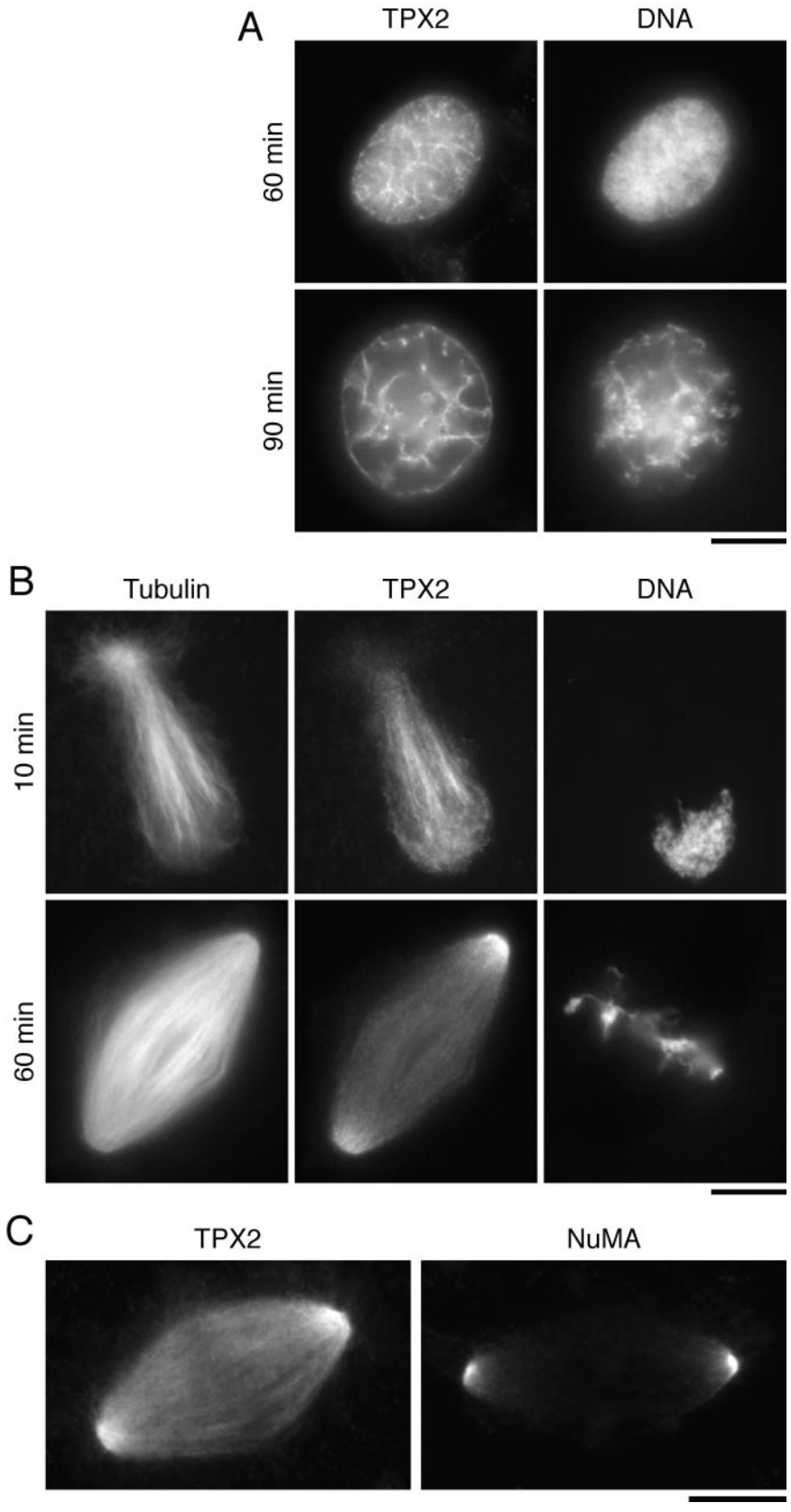

Figure 5. Immunolocalization of TPX2 in *Xenopus* egg extract. (A) Sperm nuclei were incubated in extract released into interphase by the addition of calcium for the indicated time, fixed and sedimented onto coverslips. (B) Mitotic spindles assembled in the presence of rhodamine-labeled tubulin in cycled CSF-extract. Reactions were fixed at the indicated times after reentry into mitosis and sedimented onto coverslips. Spindles and nuclei were stained with 3 μg/ml anti-TPX2N, a Cy2-labeled anti–rabbit antibody and Hoechst 33258. TPX2 localizes to a branched structure in interphase nuclei and migrates to the spindle poles in mitosis. (C) Mitotic spindles centrifuged onto coverslips, postfixed in cold methanol and stained for either TPX2 or NuMA. Images were taken under identical conditions. Bars, 10 μm.

cipitations either, suggesting that microtubules are required for the binding of Xklp2 to TPX2.

We then analyzed mitotic structures formed in TPX2-depleted extracts. TPX2 depletion did not significantly affect the formation of bipolar microtubule arrays. 1 h after cycling back into mitosis the total number of bipolar structures formed in control- and TPX2-depleted extract was about the same but TPX2-depleted bipolar arrays had

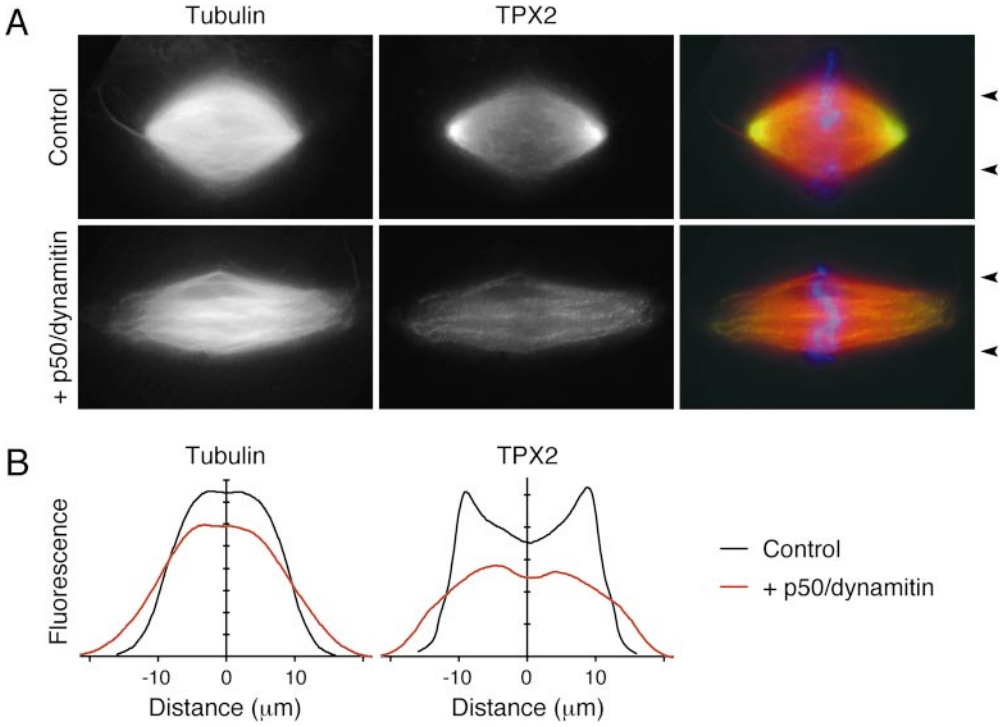

Figure 6. The dynein–dynactin complex is required for the localization of TPX2 to spindle poles. (A) Recombinant p50/dynamitin was added to cycled spindle reactions at ~0.7 mg/ml. The spindles were sedimented onto coverslips and stained with anti-TPX2N and a Cy2-conjugated anti–rabbit antibody. In the overlay, also the DNA visualized by Hoechst 33258 staining is shown in blue. Fluorescence intensity of the TPX2 staining and the rhodamine-labeled tubulin was measured in a 100-pixel wide stripe (width is indicated by arrowheads on the right) along the spindle axis. (B) The average fluorescence intensity of eleven spindles with (red) and without (black) p50/dynamitin added was plotted against the distance from the metaphase plate.

abnormal morphologies (Fig. 8, B and C). In contrast to control spindles, TPX2 staining was absent from these structures. However, more normal looking spindles often showed some remaining TPX2 staining at the poles. In general, TPX2-depleted structures appeared less compact than control spindles and displayed a variety of pole defects. Some bipolar structures had completely unfocused microtubules reminiscent of spindles formed in dynein–dynactin-inhibited extracts. Many others displayed multiple asters loosely attached to the disintegrating spindle poles (Fig. 8 C). These asters often appeared as the brightest areas indicating a reduced microtubule density. This was confirmed by quantification of the rhodamine-tubulin fluorescence in a small area between poles and metaphase plate showing that the microtubule density was reduced by ~50% in TPX2-depleted structures (Fig. 8 D). The overall size of bipolar structures assembled in TPX2-depleted extract (length 33 ± 3.4 μm, width 16 ± 3.3 μm, $n = 100$) was only marginally increased compared with control spindles (length 29 ± 3.0 μm, width 15 ± 2.1 μm, $n = 100$).

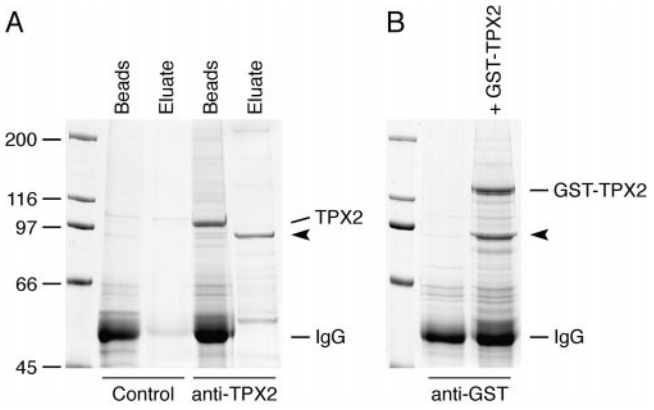

Figure 7. Immunoprecipitation of TPX2 from egg extract. (A) Immunoprecipitated proteins using a control rabbit IgG or anti-TPX2N were eluted with a high-salt buffer and proteins remaining on the beads or recovered in the eluate were analyzed on a Coomassie-stained SDS-PAGE. (B) GST-TPX2 was added to mitotic egg extract, incubated for 30 min at 20°C and immunoprecipitated with an anti-GST antibody. For both gels, the molecular mass of marker proteins is indicated on the left. A polypeptide of ~90 kD (arrowhead) is specifically immunoprecipitated together with the endogenous TPX2 or with GST-TPX2.

The TPX2 depletion phenotype could be rescued by the addition of bacterially expressed TPX2: the microtubule density in bipolar spindles formed was indistinguishable from the control and the added protein localized to the spindle poles. Most of the bipolar spindles had a normal pole morphology, but some showed open ring-like poles (Fig. 8, C and D). However, the number of bipolar structures was greatly reduced compared with control- and TPX2-depleted reactions and many monopolar and rosette-like structures formed that were not quantified due to a great variability in different experiments.

A previous analysis of Xklp2 function using the GST-Xklp2-Tail as a dominant negative inhibitor resulted predominantly in the formation of monopolar structures (Boleti et al., 1996). Since TPX2 is required for the localization of Xklp2 to the poles, we were surprised to find mostly bipolar structures in TPX2-depleted extracts. Therefore, we decided to reexamine Xklp2 function by analyzing cycled spindle assembly in Xklp2-depleted extracts. After depletion of >98% of Xklp2 from mitotic egg extract (Fig. 9 A), the percentage of normal bipolar spindles formed was indistinguishable from controls (Fig. 9 B). TPX2 remained localized to the spindle poles in Xklp2-

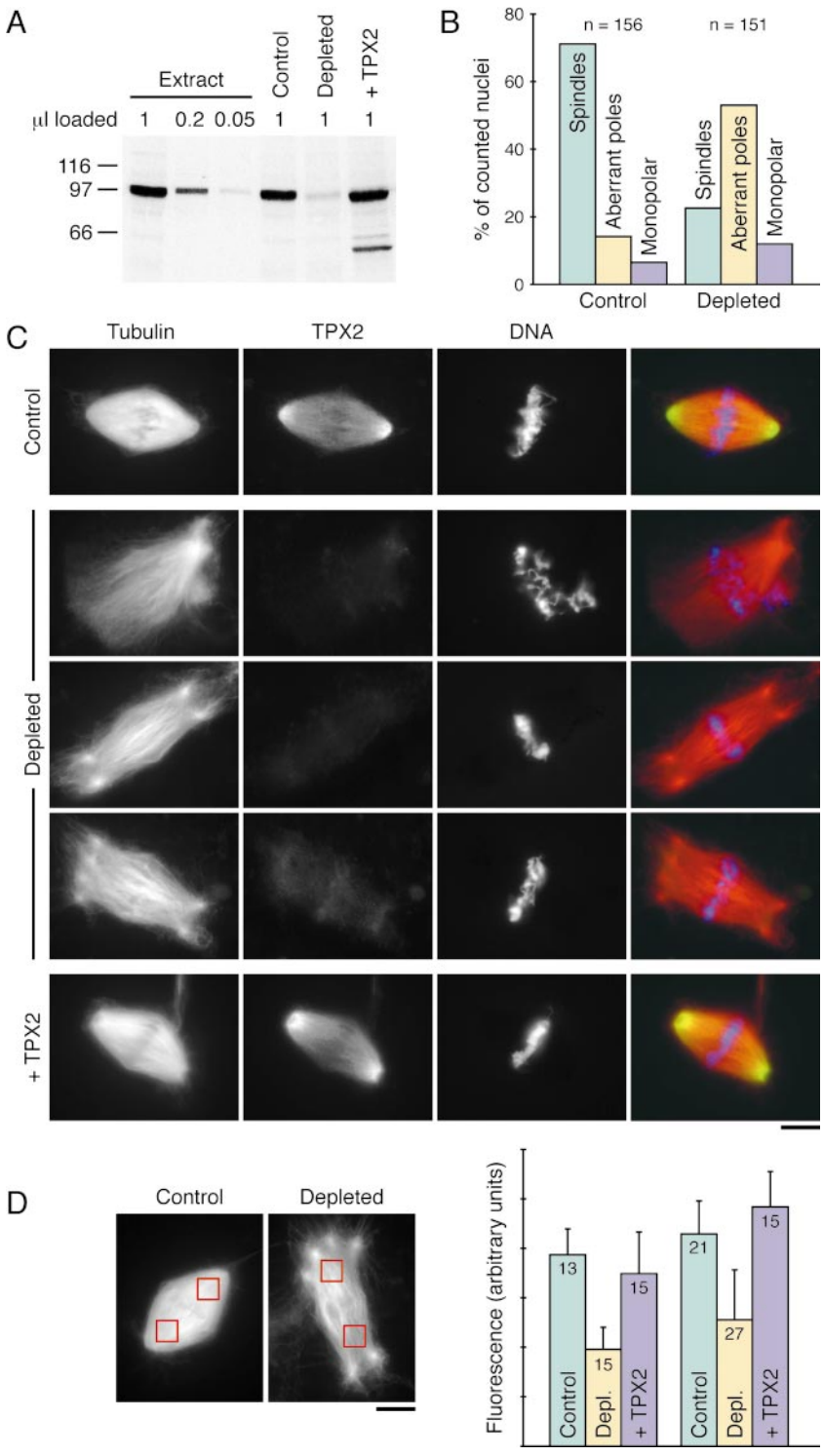

Figure 8. Depletion of TPX2 affects spindle pole structure. (A) Immunoblot probed with anti-TPX2N demonstrating the depletion efficiency. 1-, 0.2-, and 0.05-μl samples of mitotic *Xenopus* egg extract are compared with 1 μl of control- and TPX2-depleted extract supplemented with bacterially expressed TPX2. The molecular mass of marker proteins is indicated on the left. (B) Quantification of structures observed in control- and TPX2-depleted extract 1 h after cycling the extract back into mitosis. The number of quantified structures is indicated on top. (C) Representative bipolar structures observed in control- and TPX2-depleted extract supplemented with recombinant TPX2. Cycled spindles were assembled in the presence of rhodamine-labeled tubulin, fixed, centrifuged onto coverslips, and stained with anti-TPX2N and Hoechst 33258. (D) Quantification of the microtubule density in bipolar structures assembled in control- and TPX2-depleted extract supplemented with recombinant TPX2 from two independent experiments. The red boxes indicate representative areas in which the rhodamine fluorescence intensity was measured. The number of structures analyzed is shown on top of the columns. Error bars indicate the standard deviation. Bars, 10 μm.

depleted extract (Fig. 9 C). In extracts depleted of both Xklp2 and TPX2, we observed the same phenotype as when TPX2 was depleted alone (Fig. 9 C). From the immunoprecipitated material it was also evident that Xklp2 is more abundant in egg extract than TPX2 (data not shown). These experiments raised the question of the actual function of Xklp2 in spindle pole separation, but indicated that in addition to localizing Xklp2 to the poles, TPX2 plays a role in spindle pole organization.

To determine the fate of another spindle pole component when TPX2 is inhibited, TPX2-depleted structures were stained with anti-NuMA antibodies (Fig. 9 D). NuMA was clearly detectable in these structures and concentrated in the multiple microtubule foci observed in TPX2-depleted structures indicating that they may represent fragments of spindle pole material. However, the total intensity of NuMA staining was somewhat reduced compared with control spindles.

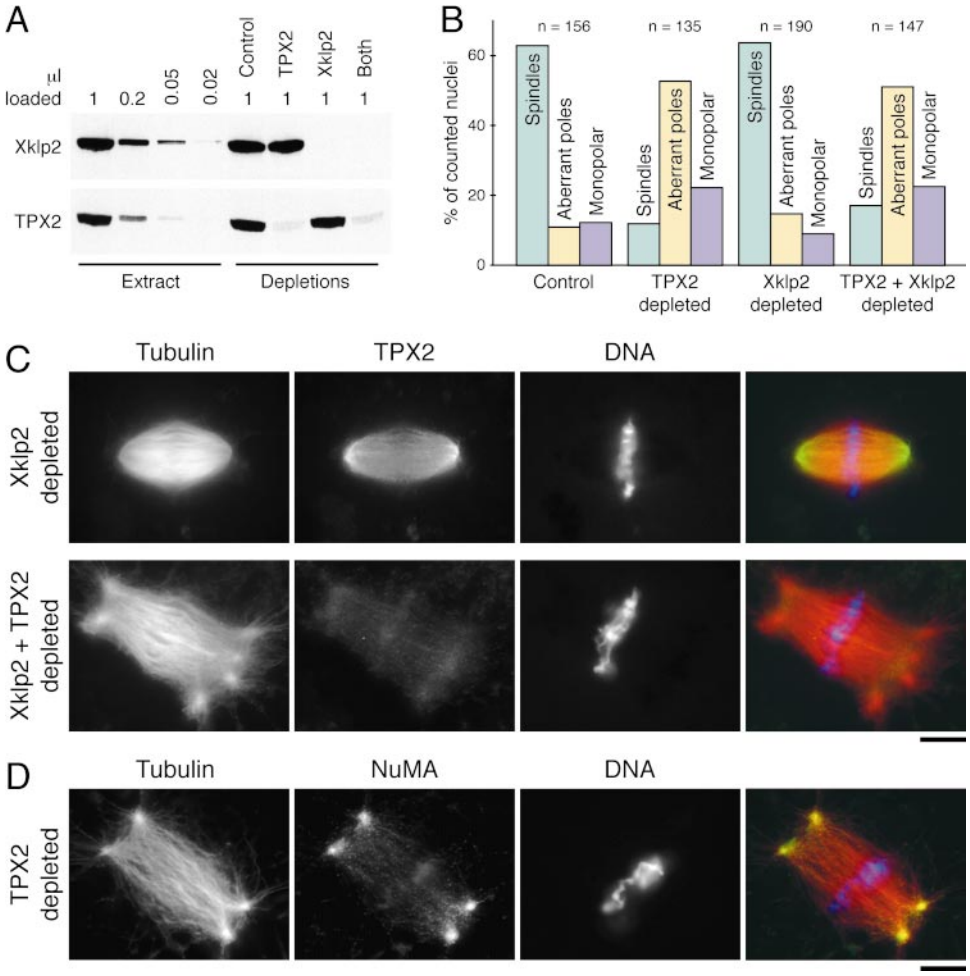

Figure 9. Cycled spindle assembly in Xklp2- and TPX2-depleted extract. (A) Immunoblot of 1-µl samples of control-, TPX2-, Xklp2-, and double-depleted extract compared with 1, 0.2, 0.05, and 0.02 µl of mitotic egg extract and probed for Xklp2 and TPX2 as indicated. (B) Quantification of structures observed under the various depletion conditions. The number of quantified structures is indicated on top. (C) Representative bipolar structures observed in Xklp2- and double-depleted extract. Cycled spindles were assembled in the presence of rhodamine-labeled tubulin, fixed, centrifuged onto coverslips and stained with anti-TPX2N and Hoechst 33258. (D) TPX2-depleted structure stained for NuMA. Bars, 10 µm.

An Excess of TPX2 Affects Spindle Pole Structure and Disrupts Bipolarity

The lack of effect of Xklp2 depletion on spindle bipolarity did not agree with the inhibition of spindle pole separation produced by the addition of GST-Xklp2-Tail (Boleti et al., 1996). Thus, we wondered whether the addition of TPX2 would have an effect similar to the addition of GST-Xklp2-Tail. Indeed, the addition of a 5–10-fold molar excess of TPX2 to cycled spindle assembly reactions resulted in a dramatic decrease of bipolar spindle formation. 60 min after reentry of the extract into mitosis, we observed a mixture of aggregated nuclei and monopolar microtubule structures that were very strongly stained by anti-TPX2 antibodies (Fig. 10, A and B). These monopolar structures were reminiscent of half-spindles observed at early time points during spindle assembly in CSF-extracts (Sawin and Mitchison, 1991a) and were comparable in length (24 ± 3.8 µm, n = 67). However, the microtubule density in these structures appeared to be extraordinarily high and they had enlarged ring-like poles. Quantification of the rhodamine-tubulin fluorescence between pole and chromatin showed that the microtubule density in the presence of excess TPX2 was increased by ~30% compared with bipolar spindles in the control reaction (Fig. 10 C). NuMA was still localized in a tight, crescent-shaped area at the poles of these monopolar structures and did not seem to overlap with the majority of TPX2 (Fig. 10 D). TPX2 addition also induced the formation of numerous ectopic asters with NuMA concentrated in the center (data not shown).

Discussion

TPX2 Is a Novel Vertebrate Spindle Pole Protein

TPX2 was identified and purified on the basis of its ability to bind to microtubules and to mediate the binding of the COOH-terminal domain of Xklp2 to microtubules in mitotic *Xenopus* egg extract (Wittmann et al., 1998). Native and recombinant TPX2 binds to microtubules with high affinity, but TPX2 has no sequence homology with other MAPs and it does not contain a tau- or CAP-Gly–like microtubule-binding motif (De Zeeuw et al., 1997; Drewes et al., 1998). However, we found that TPX2 shares homologies with predicted proteins from different vertebrate species and is highly homologous to a human protein of unknown function, fls353 or DIL-2, that is differentially expressed in different types of cancerous cells (Hufton et al., 1999; Manda et al., 1999). We did not find any homology to *Drosophila*, *C. elegans*, or yeast proteins. Thus, TPX2 defines a novel family of vertebrate MAPs. It is interesting to note that DIL-2 is predominantly expressed in

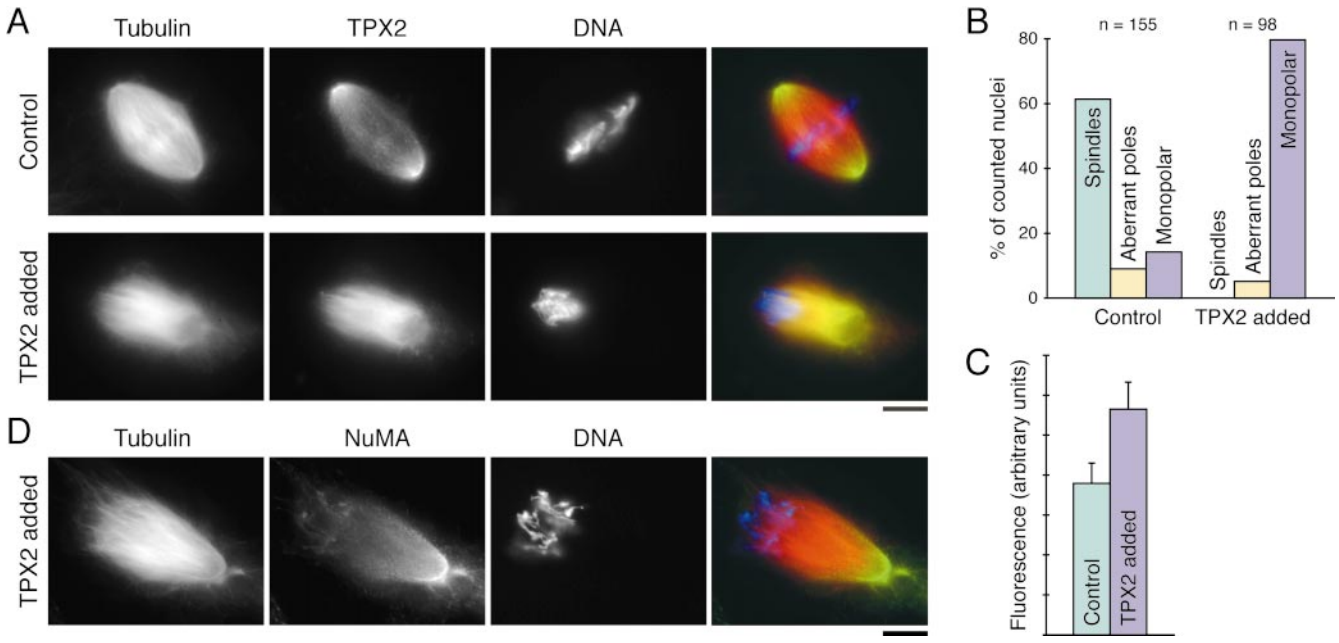

Figure 10. An excess of TPX2 prevents the formation of bipolar spindles. (A) Representative structures observed in control and TPX2-supplemented reactions. Cycled spindles were assembled in the presence of rhodamine-labeled tubulin, fixed, centrifuged onto coverslips, and stained with anti-TPX2N and Hoechst 33258. (B) Quantification of structures observed in spindle assembly reactions supplemented with either control buffer or a 5–10-fold molar excess of TPX2. The number of quantified structures is indicated on top. (C) Quantification of the microtubule density in bipolar control spindles and in monopolar structures in TPX2-supplemented reactions. Error bars indicate the standard deviation ($n = 20$). (D) Monopolar structure in the presence of excess TPX2 stained for NuMA. Bars, 10 μm.

fetal tissues consistent with a function in cell division (Manda et al., 1999).

TPX2 shows a dynamic localization during the cell cycle, accumulating at spindle poles during mitosis. In interphase, it is nuclear like other mitotic MAPs or certain centrosomal proteins (Oegema et al., 1995, 1997; Merdes et al., 1996; Andersen and Karsenti, 1997) and in nuclei assembled in egg extracts, TPX2 associates with a branched intranuclear structure. Since in TPX2-depleted extracts, interphase nuclei form without any visible defect and the chromatin condenses normally upon entry into mitosis, TPX2 is unlikely to have a nuclear function. A lack of nuclear phenotype has also been observed in NuMA depletions (Merdes and Cleveland, 1998). This suggests that nuclear import of spindle pole components may be merely a way to sequester them from the cytoplasm during interphase.

TPX2 Is a Mitotic Phosphoprotein

The TPX2 sequence contains a number of potential phosphorylation sites for cdc2 and MAP kinase. TPX2 is indeed phosphorylated in mitotic versus interphase extract and mitotic phosphorylation is stimulated by polymerization of microtubules. NuMA is the only other protein where something similar has been observed (Gaglio et al., 1995). While in many cases the affinity of MAPs for microtubules is downregulated by phosphorylation (Andersen et al., 1994; Drewes et al., 1997), phosphorylated TPX2 purified from egg extract as well as the unphosphorylated bacterially expressed protein bind to microtubules in biochemical assays.

Using mass spectrometry we have been able to detect that at least one of the cdc2 sites and all of the MAP kinase sites can be phosphorylated in egg extract (Wittmann, T., G. Neubauer, and M. Wilm, unpublished results). Furthermore, the conservation of some of the phosphorylation sites throughout a number of vertebrate TPX2 homologues (Fig. 1 C) suggests that these sites are functionally relevant. Since it has recently been shown that activated MAP kinase localizes to kinetochores and mitotic spindle poles (Shapiro et al., 1998; Zecevic et al., 1998), it is possible that some aspects of TPX2 function are regulated by MAP kinase.

Targeting of Motor Proteins

The mechanisms by which kinesin motor proteins are targeted to, anchored, and activated at specific cellular locations appear to be complex and are still largely unknown (for a recent review see Goldstein and Philp, 1999). In this paper, we have demonstrated that TPX2 is required for the localization of Xklp2 to microtubule minus ends during mitosis. We were also able to reconstitute the binding of the COOH-terminal domain of Xklp2 to microtubules using purified components. Thus, the targeting of Xklp2 requires some sort of direct interaction between Xklp2 and TPX2. We do not yet understand the exact nature of this interaction but it probably involves the COOH-terminal leucine zipper domain of Xklp2 (Wittmann et al.,

1998). However, in the microtubule-binding assay only a fraction of the Xklp2 COOH-terminal domain binds to TPX2 and microtubules indicating a rather low affinity of Xklp2 for TPX2. In addition, we never succeeded to isolate a TPX2–Xklp2 complex by immunoprecipitation or other means, indicating that microtubules are required for this interaction to occur at all. Determining which domains of TPX2 are involved in microtubule and Xklp2 binding may provide some insights about how this ternary complex is assembled.

Addition of antibodies against Xklp2 or the dominant negative GST-Xklp2-Tail protein to egg extracts inhibited spindle assembly resulting in mainly monopolar structures (Boleti et al., 1996). Since TPX2 is required for the localization of Xklp2 to spindle poles we expected that delocalization of Xklp2 by immunodepletion of TPX2 would have a similar phenotype. However, TPX2 depletion does not have a significant effect on spindle bipolarity leading us to reexamine the previous interpretation of Xklp2 function. We now find that depletion of Xklp2 from egg extracts does not prevent the formation of bipolar spindles. Xklp2 is not essential either to organize a bipolar spindle around chromatin beads (Walczak et al., 1998). Thus, there are two possibilities: (a) Xklp2 is not required for spindle assembly and the previously observed inhibition of bipolarity by the addition of GST-Xklp2-Tail is not due to a direct interference with Xklp2-function; (b) Xklp2 function in spindle assembly is redundant, and the removal of Xklp2 but not the addition of a dominant negative mutant can be compensated for by other motor proteins like Eg5. Nonetheless, Xklp2 may have a mitotic function since injection of Xklp2 antisense oligonucleotides into *Xenopus* oocytes blocks the early mitotic divisions (Robb et al., 1996).

Role of TPX2 in Spindle Pole Organization

TPX2 has other functions in addition to targeting Xklp2 to the poles. Immunodepletion of TPX2 results in the formation of bipolar spindles with abnormal morphologies and disintegrating poles often with bright foci of microtubules loosely attached. These foci still contain NuMA, however, it is unclear whether they represent intact centrosomes, fragments of nucleating material or centers of self-organized asters. In addition, TPX2-depleted structures have a reduced density of microtubules between poles and chromatin. These results indicate that TPX2 is involved in stabilizing the spindle and/or spindle poles. However, it is possible that the pole defects are an indirect consequence of a weakened spindle structure.

An excess of TPX2 blocks the formation of bipolar spindles and leads to an abnormally enlarged pole structure very similar to those formed after addition of GST-Xklp2-Tail (Boleti et al., 1996). This suggests that the addition of an excess of a pole component may stabilize the poles in such a way that bipolarity cannot be established anymore. Interestingly, in these monopolar structures, NuMA still localizes to a very tight area around the pole indicating that the overall organization of pole proteins may still be intact.

NuMA and the dynein–dynactin complex are key players in spindle pole formation. Inhibition of any of these molecules severely affects spindle pole integrity resulting in bipolar arrays with unfocused, frayed poles (Merdes et al., 1996; Heald et al., 1997). Interestingly, both NuMA and TPX2 require cytoplasmic dynein for their localization to spindle poles. Whereas NuMA binds directly to the dynein–dynactin complex (Merdes et al., 1996), we could not detect a direct interaction of TPX2 with either dynein–dynactin or NuMA, but we cannot rule out a transient interaction of TPX2 with these molecules. Thus, the two models that we proposed previously for the mechanism of localization of TPX2/Xklp2 to microtubule minus ends during mitosis, a direct interaction of TPX2 with dynein–dynactin versus a microtubule affinity-regulating gradient along the spindle axis (Wittmann et al., 1998), are still possible and the exact mechanism remains to be elucidated.

It has become clear over the last few years that spindle poles are fundamentally different from centrosomes and that centrosomes are in fact not required for the formation of a bipolar spindle (Heald et al., 1996; Khodjakov et al., 1999). It has been suggested that NuMA provides a structural framework at the pole, cross-linking microtubules in a centrosome-independent way (Compton, 1998; Dionne et al., 1999). Although the primary structures of TPX2 and NuMA are completely unrelated, both proteins appear to have overlapping functions leading us to propose that TPX2 is essential for proper assembly of vertebrate mitotic spindle poles.

We would like to thank all members of the Karsenti and Hyman labs for helpful discussions, especially Andrei Popov and Célia Antonio for communal extracts, as well as Nathalie Le Bot and Arshad Desai for critical reading and comments on the manuscript. Special thanks go to Hironori Funabiki and Arshad Desai for the hint about the protein A dynabeads and to Andreas Merdes for anti-NuMA antibodies. We also thank the members of the EMBL mass spectrometry and protein sequencing facility, Gitte Neubauer, Angela Bachi, and Keith Ashman.

Submitted: 23 March 2000
Revised: 24 May 2000
Accepted: 26 May 2000

References

Andersen, S.S.L. 2000. Spindle assembly and the art of regulating microtubule dynamics by MAPs and stathmin/Op18. *Trends Cell Biol.* 10:261–267.

Andersen, S.S.L., and E. Karsenti. 1997. XMAP310: A *Xenopus* rescue-promoting factor localized to the mitotic spindle. *J. Cell Biol.* 139:975–983.

Andersen, S.S.L., B. Buendia, J.E. Domínguez, A. Sawyer, and E. Karsenti. 1994. Effect on microtubule dynamics of XMAP230, a microtubule-associated protein present in *Xenopus laevis* eggs and dividing cells. *J. Cell Biol.* 127:1289–1299.

Ausubel, F., R. Brent, R.E. Kingston, D.D. Moore, J.G. Seidman, J.A. Smith, and K. Struhl. 1995. Short Protocols in Molecular Biology. John Wiley & Sons, Inc., New York.

Boleti, H., E. Karsenti, and I. Vernos. 1996. Xklp2, a novel *Xenopus* centrosomal kinesin-like protein required for centrosome separation during mitosis. *Cell.* 84:49–59.

Carazo-Salas, R.E., G. Guarguaglini, O.J. Gruss, A. Segref, E. Karsenti, and I.W. Mattaj. 1999. Generation of GTP-bound Ran by RCC1 is required for chromatin-induced mitotic spindle formation. *Nature.* 400:178–181.

Cassimeris, L. 1999. Accessory protein regulation of microtubule dynamics throughout the cell cycle. *Curr. Opin. Cell Biol.* 11:134–141.

Compton, D.A. 1998. Focusing on spindle poles. *J. Cell Sci.* 111:1477–1481.

De Zeeuw, C.I., C.C. Hoogenraad, E. Goedknegt, E. Hertzberg, A. Neubauer, F. Grosveld, and N. Galjart. 1997. CLIP-115, a novel brain-specific cytoplasmic linker protein, mediates the localization of dendritic lamellar bodies. *Neuron.* 19:1187–1199.

Desai, A., A. Murray, T.J. Mitchison, and C.E. Walczak. 1999. The use of *Xenopus* egg extracts to study mitotic spindle assembly and function in vitro. *Methods Cell Biol.* 61:385–412.

Dionne, M.A., L. Howard, and D.A. Compton. 1999. NuMA is a component of an insoluble matrix at mitotic spindle poles. *Cell Motil. Cytoskeleton.* 42:189–203.

Drewes, G., A. Ebneth, U. Preuss, E.-M. Mandelkow, and E. Mandelkow. 1997. MARK, a novel family of protein kinases that phosphorylate microtubule-associated proteins and trigger microtubule disruption. *Cell*. 89:297–308.

Drewes, G., A. Ebneth, and E.-M. Mandelkow. 1998. MAPs, MARKs and microtubule dynamics. *Trends Biochem. Sci.* 23:307–311.

Endow, S.A. 1999. Microtubule motors in spindle and chromosome motility. *Eur. J. Biochem*. 262:12–18.

Gaglio, T., A. Saredi, and D.A. Compton. 1995. NuMA is required for the organization of microtubules into aster-like mitotic arrays. *J. Cell Biol.* 131:693–708.

Gaglio, T., M.A. Dionne, and D.A. Compton. 1997. Mitotic spindle poles are organized by structural and motor proteins in addition to centrosomes. *J. Cell Biol.* 138:1055–1066.

Goldstein, L.S.B., and A.V. Philp. 1999. The road less traveled: Emerging principles of kinesin motor utilization. *Annu. Rev. Cell Dev. Biol.* 15:141–183.

Heald, R., and C.E. Walczak. 1999. Microtubule-based motor function in mitosis. *Curr. Opin. Struct. Biol.* 9:268–274.

Heald, R., R. Tournebize, T. Blank, R. Sandaltzopoulos, P. Becker, A. Hyman, and E. Karsenti. 1996. Self-organization of microtubules into bipolar spindles around artificial chromosomes in *Xenopus* egg extracts. *Nature*. 382: 420–425.

Heald, R., R. Tournebize, A. Habermann, E. Karsenti, and A. Hyman. 1997. Spindle assembly in *Xenopus* egg extracts: Respective roles of centrosomes and microtubule self-organization. *J. Cell Biol.* 138:615–628.

Heald, R., R. Tournebize, I. Vernos, A. Murray, T. Hyman, and E. Karsenti. 1998. In vitro assays for mitotic spindle assembly and function. *In* Cell Biology: A Laboratory Handbook. Vol. 2. J.E. Celis, editor. Academic Press, San Diego, CA. 326–335.

Heck, M.M. 1999. Dr. Dolittle and the making of the mitotic spindle. *Bioessays*. 21:985–990.

Hufton, S.E., P.T. Moerkerk, R. Brandwijk, A.P. de Bruine, J.-W. Arends, and H.R. Hoogenboom. 1999. A profile of differentially expressed genes in primary colorectal cancer using suppression subtractive hybridization. *FEBS Lett.* 463:77–82.

Hyman, A.A., D. Drechsel, D. Kellogg, S. Salser, K. Sawin, P. Steffen, L. Wordeman, and T.J. Mitchison. 1991. Preparation of modified tubulins. *Methods Enzymol.* 196:478–485.

Kalab, P., R.T. Pu, and M. Dasso. 1999. The Ran GTPase regulates mitotic spindle assembly. *Curr. Biol.* 9:481–484.

Khodjakov, A., R.W. Cole, B.R. Oakley, and C.L. Rieder. 1999. Centrosome-independent mitotic spindle formation in vertebrates. *Curr. Biol.* 10:59–67.

Khodjakov, A., and C.L. Rieder. 1999. The sudden recruitment of γ-tubulin to the centrosome at the onset of mitosis and its dynamic exchange throughout the cell cycle, do not require microtubules. *J. Cell Biol.* 146:585–596.

Manda, R., T. Kohno, Y. Matsuno, S. Takenoshita, H. Kuwano, and J. Yokota. 1999. Identification of genes (SPON2 and C20orf2) differentially expressed between cancerous and noncancerous lung cells by mRNA differential display. *Genomics*. 61:5–14.

Merdes, A., and D.W. Cleveland. 1998. The role of NuMA in the interphase nucleus. *J. Cell Sci.* 111:71–79.

Merdes, A., R. Heald, K. Samejima, W.C. Earnshaw, and D.W. Cleveland. 2000. Formation of spindle poles by dynein/dynactin-dependent transport of NuMA. *J. Cell Biol.* 149:851–862.

Merdes, A., K. Ramyar, J.D. Vechio, and D.W. Cleveland. 1996. A complex of NuMA and cytoplasmic dynein is essential for spindle assembly. *Cell*. 87: 447–458.

Murray, A.W. 1991. Cell cycle extracts. *Methods Cell Biol.* 36:581–605.

Oegema, K., W.F. Marshall, J.W. Sedat, and B.M. Alberts. 1997. Two proteins that cycle asynchronously between centrosomes and nuclear structures: *Drosophila* CP60 and CP190. *J. Cell Sci.* 110:1573–1583.

Oegema, K., W.G.F. Whitfield, and B. Alberts. 1995. The cell cycle-dependent localization of the CP190 centrosomal protein is determined by the coordinate action of two separable domains. *J. Cell Biol.* 131:1261–1273.

Robb, D.L., J. Heasman, J. Raats, and C. Wylie. 1996. A kinesin-like protein is required for germ plasm aggregation in *Xenopus*. *Cell*. 87:823–831.

Sawin, K.E., and T.J. Mitchison. 1991a. Mitotic spindle assembly by two different pathways in vitro. *J. Cell Biol.* 112:925–940.

Sawin, K.E., and T.J. Mitchison. 1991b. Poleward microtubule flux in mitotic spindles assembled in vitro. *J. Cell Biol.* 112:941–954.

Shapiro, P.S., E. Vaisberg, A.J. Hunt, N.S. Tolwinski, A.M. Whalen, J.R. McIntosh, and N.G. Ahn. 1998. Activation of the MKK/ERK pathway during somatic cell mitosis: direct interactions of active ERK with kinetochores and regulation of the mitotic 3F3/2 phosphoantigen. *J. Cell Biol.* 142:1533–1545.

Shevchenko, A., M. Wilm, O. Vorm, and M. Mann. 1996. Mass spectrometric sequencing of proteins from silver-stained polyacrylamide gels. *Anal. Chem*. 68:850–858.

Stearns, T., and M. Kirschner. 1994. In vitro reconstitution of centrosome assembly and function: The central role of γ-tubulin. *Cell*. 76:623–637.

Tuma, M.C., A. Zill, N. Le Bot, I. Vernos, and V. Gelfand. 1998. Heterotrimeric kinesin II is the microtubule motor protein responsible for pigment dispersion in *Xenopus* melanophores. *J. Cell Biol.* 143:1547–1558.

Vernos, I., and E. Karsenti. 1996. Motors involved in spindle assembly and chromosome segregation. *Curr. Opin. Cell Biol.* 8:4–9.

Walczak, C.E., S. Verma, and T.J. Mitchison. 1997. XCTK2: A kinesin-related protein that promotes mitotic spindle assembly in *Xenopus laevis* egg extracts. *J. Cell Biol.* 136:859–870.

Walczak, C.E., I. Vernos, T.J. Mitchison, E. Karsenti, and R. Heald. 1998. A model for the proposed roles of different microtubule-based motor proteins in establishing spindle bipolarity. *Curr. Biol.* 8:903–913.

Waterman-Storer, C.M., A. Desai, J.C. Bulinski, and E.D. Salmon. 1998. Fluorescent speckle microscopy, a method to visualize the dynamics of protein assemblies in living cells. *Curr. Biol.* 8:1227–1230.

Wilde, A., and Y. Zheng. 1999. Stimulation of microtubule aster formation and spindle assembly by the small GTPase Ran. *Science*. 284:1359–1362.

Wilm, M., and M. Mann. 1996. Analytical properties of the nanoelectrospray ion source. *Anal. Chem*. 68:1–8.

Wittmann, T., and T. Hyman. 1999. Recombinant p50/dynamitin as a tool to examine the role of dynactin in intracellular processes. *Methods Cell Biol.* 61: 137–143.

Wittmann, T., H. Boleti, C. Antony, E. Karsenti, and I. Vernos. 1998. Localization of the kinesin-like protein Xklp2 to spindle poles requires a leucine zipper, a microtubule-associated protein, and dynein. *J. Cell Biol.* 143:673–685.

Zecevic, M., A.D. Catling, S.T. Eblen, L. Renzi, J.C. Hittle, T.J. Yen, G.J. Gorbsky, and M.J. Weber. 1998. Active MAP kinase in mitosis: localization at kinetochores and association with the motor protein CENP-E. *J. Cell Biol.* 142:1547–1558.